

Torsion modulus with CaCO₃ fillers in unsaturated polyester resin - mechanical spectroscopy

Carlos Alberto Fonzar Pintão^{1*} , Airton Baggio² , Lucas Pereira Piedade² ,
Luiz Eduardo de Angelo Sanchez²  and Gilberto de Magalhães Bento Gonçalves² 

¹*Departamento de Física, Faculdade de Ciências, Universidade Estadual Paulista – UNESP, Bauru, SP, Brasil*

²*Departamento de Engenharia Mecânica, Universidade Estadual Paulista – UNESP, Bauru, SP, Brasil*

*carlos.fonzar@unesp.br

Abstract

This work presents an alternative to studying and determining the torsion modulus, G, in composites. For this purpose, we use a measuring system with a rotation motion sensor coupled with a torsion pendulum that allows for determining the angular position as a function of the time. Then, through an equation derived from mechanical spectroscopy studies that permits the calculation of G's value, the experiments focus on samples of different quantities of calcium carbonate (CaCO₃) in unsaturated polyester resins. The results show that CaCO₃ (33.33%W) fillers increase G's value by 88% compared with unsaturated resin (100%W). Furthermore, there is a density increase of approximately 21% with the addition of CaCO₃, considering the same two samples, which makes these composites the most massive. The relationship between G and composite density shows that it is possible to change the amount of CaCO₃ to increase torsion resistance values in a controlled way.

Keywords: *calcium carbonate, mechanical spectroscopy, polyester resin, torsion modulus.*

How to cite: Pintão, C. A. F., Baggio, A., Piedade, L. P., Sanchez, L. E. A., & Gonçalves, G. M. B. (2022). Torsion modulus with CaCO₃ fillers in unsaturated polyester resin - mechanical spectroscopy. *Polímeros: Ciência e Tecnologia*, 32(2), e2022013. <https://doi.org/10.1590/0104-1428.20210105>

1. Introduction

It is necessary to know material behavior when subjected to stresses or loads to determine the most appropriate application. Therefore, the elastic modulus, which measures a material's rigidity, must always be considered. It represents an essential property in the behavior of materials used in various applications such as aerospace^[1,2], automotive^[3], naval^[4], civil^[5], electrical^[6,7], biomedical^[8], implants^[9], and structures^[10-12] subjected to torsion and traction (compression). The elastic modulus, reported for metals and their alloys, depends on the atomic bonds and the distances between atoms in the crystalline lattice. Therefore, it is sensitive to the addition of elements, thermomechanical treatments, and deformation processing. However, composites have amorphous and crystalline parts and form with different additives or fillers. Thus, it is not simple to establish a general pattern of the influence of these same factors that consider metals and their impact on the elastic modulus.

Polymer additives are auxiliary added components. Their inclusion in polymer formulations or compositions is intended for specific applications^[13-15], such as modifying and improving properties, reducing cost, or facilitating processing. Essential polymer additives include mineral inorganic fillers, plasticizers, dyes, antioxidants, ultraviolet absorbers, flame retardants, thermal stabilizers, blowing agents, flavoring agents, antifungals, and impact modifiers.

In composites, adding mineral fillers can weaken polymers, although their stiffness increases. The efforts of several authors have improved the properties of materials with the addition of inorganic fillers such as silicon dioxide^[16], zinc oxide^[17], calcium carbonate (CaCO₃)^[18], and carbon fibers^[19]. Calcium carbonate is the second most used mineral material after talc. The use of CaCO₃ with adequate hardness (Mohs ~3 hardness) does not cause short-term machine processing failures^[20]. Calcium carbonate reduces some of the cost without affecting properties. For polymer composites, adhesion between the filler and matrix is essential. Suppose adherence is active at the interface, the modulus, stiffness, and strength of a particulate composite increase. Some authors^[21-23] have directed attention to investigating CaCO₃ nanofiller polypropylene compounds. However, they have yet to advance the creep-limiting properties of CaCO₃ nanofiller polypropylene compounds.

Although Young's modulus is low for plastics and never constant compared with that of metals, deflection resistance (stiffness) is often a concern with the use of plastics. The rigidity of a structure depends on the values from the elastic modulus and the geometry of the materials. Thus, there are no data on the torsion modulus in composites. This work aims to study the influence of additives such as CaCO₃ in unsaturated polyester resins. Then, we want to

establish a relationship between the torsion modulus and the quantity of CaCO_3 .

Traditionally, the static (stress-strain curves) or dynamic (ultrasound or vibration) methods^[24,25] determine the elastic modulus. In this paper, the modulus of elasticity's behavior to torsion G by an alternative technique to the traditional that is nondestructive and using mechanical spectroscopy allows for studying the effects of CaCO_3 additives. Furthermore, to apply the technique, it is unnecessary to know the Poisson's ratio of the sample.

2. Materials and Methods

2.1 Materials

Ashland manufactured the resin used to manufacture the specimens and classified it as unsaturated polyester resin under trade reference Arazyn 13.0. Calcium carbonate, known as calcite, is one of the most abundant minerals in nature. It is a chemical of formula CaCO_3 and the main component of rocks such as limestone. The particle size is 325 mesh, and its density is between 2.70 and 2.85 g/cm^3 . For better use of torsion test equipment, the specimens are formed in round bars with a 5.0 mm diameter and a length of 130 mm.

The device for creating the samples constructed from a glass fiber-reinforced polyester resin mold with an isophthalic gel coat surface provides a smooth surface on the specimens and ensures the samples' dimensional standardization. The mold has dimensions of 120 mm x 220 mm x 80 mm, a hole diameter of 5.0 mm, and guides for opening in two parts, as shown in Figure 1.

We adopted the following terminology in our mix of resin and additives for the specimens: CP-00 represents a reference specimen. Samples with 100% resin and their values serve as parameters for the other combinations' results. Calcium carbonate was added to different models (CP-11 to CP-20), ranging from 5 in 5 parts by weight to every 100 pieces by weight of the resin. Due to its high density, a composition of over 50 elements by weight represents a pasty mixture

with little use in composite parts manufacturing processes. Table 1 summarizes the composition of resin with additive characteristics of these specimens.

2.2 Methods

2.2.1 Method for measurement torsion modulus, G

The mechanical spectroscopy technique to determine G 's value has been studied in our laboratories and can be used to investigate changes in these materials' mechanical properties. Therefore, the method for determining G is brief here. It consists of one torsion pendulum that can be adjusted to set its inertia to different values (in our case, four different values were used) and register its angular position θ concerning an axis of rotation as a function of time t . For this purpose, we used a rotational movement sensor (RMS; see Figure 2).

Mechanical spectroscopy^[25] (i.e., the torsion motion of the pendulum) is described by the

$$I \frac{d^2\theta}{dt^2} + G_0(1 + i \tan \varphi)\theta = 0 \quad (1)$$

The symbols I , G_0 , and i represent the rotational inertia, the torsion constant of the sample fixed to the pendulum, and the imaginary number, respectively. In this case, we assume that air resistance and the friction of the RMS and rotational system (RS) bearings are negligible because they should not significantly influence movement^[26]. The solution to Equation 1 takes the form $\theta = \theta_0 e^{i\omega^*t}$, where $\omega^* = \omega_0 \left(1 + i \frac{\delta}{2\pi}\right)$ and $\tan \varphi = \frac{\delta}{\pi}$. We express G_0 as

$$G_0 = I \omega_0^2 \left(1 - \frac{\delta^2}{4\pi^2}\right) \quad (2)$$

This equation suggests that the moment of inertia of the pendulum I , the angular velocity ω_0 , and the term $\frac{\delta}{2\pi}$ permit G_0 . It is possible to alter the masses or their position on the pendulum's torsion rod, which changes I and modifies the

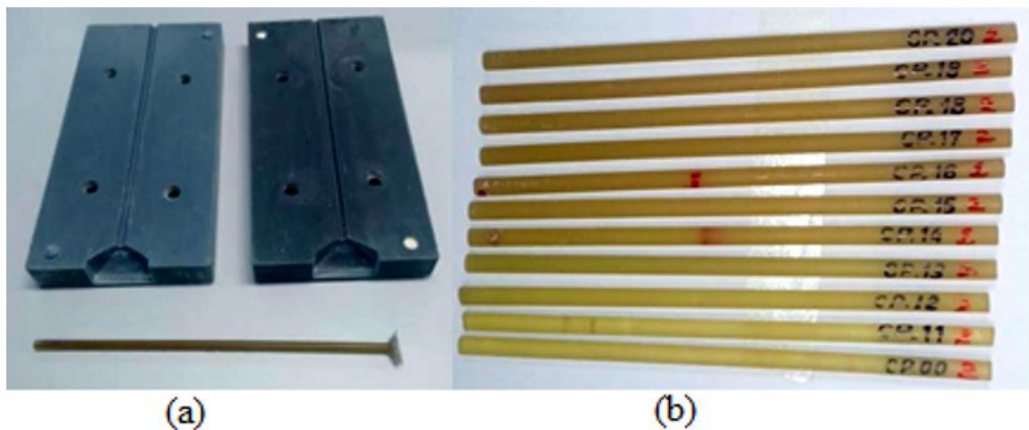


Figure 1. (a) Matrix used for making the samples and photo of one; (b) Samples: CP-00, reference with 100%W resin. CP-11 to CP-20, addition of CaCO_3 , ranging from 5 in 5 parts by weight to every 100 parts by weight of the resin.

Table 1. Composition of resin with additive.

Samples	Contraction linear post-cure (mm/m)	Resin Part by weight	Resin Percentage (%)	CaCO ₃ Part by weight	CaCO ₃ Percentage (%)	Before catalysis ρ(g/cm ³)	After catalysis ρ(g/cm ³)
CP-00	26.1	100	100.00	---	---	1.10	1.18
CP-11	26.2	100	95.24	5	4.76	1.13	1.23
CP-12	25.1	100	90.91	10	9.09	1.17	1.26
CP-13	24.4	100	86.96	15	13.04	1.22	1.28
CP-14	21.6	100	83.33	20	16.67	1.26	1.30
CP-15	24.7	100	80.00	25	20.00	1.31	1.32
CP-16	18.6	100	76.92	30	23.08	1.34	1.34
CP-17	21.7	100	74.07	35	25.93	1.36	1.38
CP-18	20.4	100	71.43	40	28.57	1.38	1.40
CP-19	18.9	100	68.97	45	31.03	1.40	1.41
CP-20	17.2	100	66.67	50	33.33	1.42	1.43

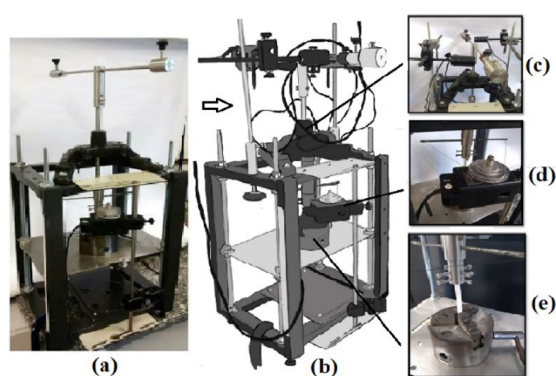


Figure 2. Measurement system: (a) Complete view of the system without electromagnets; (b) complete drawing of the artistic design of the system in 2D; (c) electromagnets setup; (d) detailed view of the RMS; (e) sample fixation.

value of ω_0 . Then, G_0 depends on the oscillation system's frequency, and we can obtain a dynamic measurement. For small angles of oscillation, in which the measuring system has a linear behavior, we can express G_0 as

$$G_0 = \frac{\text{applied torque}}{\theta} \quad (3)$$

because the main objective is to determine the torsion modulus G . We used a solid sample with a uniform circular transversal section of diameter d and length L .

Therefore, we can calculate the resistive torque when considering material problems^[27]. The sample is submitted when it undergoes torsion through a torque applied by a pendulum (see Figure 1). The following equation calculates this torque:

$$\text{resistive torque} = T_R = \frac{G J_C \theta}{L} \quad (4)$$

Where J_C is the polar moment of inertia of the cross-section. Then, the equation is

$$J_C = \frac{\pi d^4}{32} \quad (5)$$

If there is static equilibrium (i.e., the applied torque is the same as the resistive torque), we can combine Equations 3 and 4 to give

$$G_0 = \frac{G J_C}{L} \quad (6)$$

Thus, the magnitude of G results by substituting Equation 2 into (6). As a result,

$$G = \frac{L}{J_C} G_0 = \frac{L}{J_C} I \omega_0^2 \left(1 - \frac{\delta^2}{4 \pi^2} \right) \quad (7)$$

Equation 7 is validated in the article^[28], where we show that G can change with the length (L) and diameter (d) of the sample. However, the experimental values found for CP-Ti are practically the same as those in the literature^[27,29].

Authors^[28,30] have validated Equation 7; now, it is applied to a composite material, which is a different situation than that of a homogeneous material (CP-Ti). Therefore, it is necessary to validate it for this case. If we replace $\omega^* = \omega_0 \left(1 + i \frac{\delta}{2 \pi} \right)$ in the solution $\theta = \theta_0 e^{i \omega^* t}$, relative to the differential equation that describes the motion of the free pendulum as given above, then

$$\theta = \theta_0 e^{-\frac{\delta}{2 \pi} \omega_0 t} (\cos \omega_0 t + i \sin \omega_0 t) \quad (8)$$

In Equation 8, taking the real number part gives the following equation:

$$\theta = \theta_0 e^{-\frac{\delta}{T_0} t} \cos \omega_0 t \quad (9)$$

The parameters δ and ω_0 obtained from the experimental θ versus t curve were determined using the RMS software and the Pasco interface for given L , d , and I values. A fit function similar to Equation 9 was used with Origin 7.0 software by selecting a "waveform" function such as the following:

$$\varphi = A e^{-\frac{t}{t_0}} \sin \left(\frac{\pi}{W} t - \frac{\pi}{W} t_C \right) \quad (10)$$

By comparing this equation with Equation 9, we can consider the parameters t_0 and W , as obtained by fitting Equation 10 to the experimental values, and we are then able to get the parameters δ and ω_0 :

$$T = \frac{2 \pi}{\omega_0} = 2W \quad \text{and} \quad \delta = \frac{2W}{t_0} \quad (11)$$

Then, using Equation 7, we determined G and the total internal friction of the system $Q_T^{-1} = \frac{\delta}{2\pi}$.

2.2.2 Acquisition method for the moment of inertia (I)

Our research laboratory's method determined the torsion pendulum's rotational inertia^[26,31]. First, we determined the torsion pendulum's inertia moment (I) by removing the sample and the electromagnetic system (see Figure 1). The literature describes several techniques to determine the momentum of inertia of a body; however, the one closest to the measurements performed stands out in this work^[32]. Then, we adopted the same procedure as the cited authors. The resulting torque (τ) responsible for the rotational movement of the measured pendulum system is

$$\tau = \tau_T - \tau_F = I \alpha_0 \quad (12)$$

Here, τ_f is the torque of the friction force acting on the rotating shaft, whereas I and α_0 are the inertia moment and the pendulum's angular acceleration, respectively. It must be remembered that the torque of the traction force is $\tau_T = m(g - \alpha_0 r)r$, where $r = (18.75 \pm 0.03)10^{-3}$ m and $g = (9.79 \pm 0.01)$ m/s². With Equation 12, we can show that the inclination equals I .

2.2.3 Scanning electron microscopy (SEM)

We realized SEM on a Zeiss model EVO LS1. Samples were coated with gold for visualization using the sputtering technique^[33]. We made measurements in a high vacuum (10^{-3} Pa) with a magnification of 500 X and 5.0 kX of a transversal section of the sample bar's internal region. The aim was to visualize the $CaCO_3$ incorporated into the samples: CP-00 reference with 100%W in resin. CP-11 to CP-20 had $CaCO_3$ added, ranging from 5 in 5 parts by weight to every 100 parts by weight of the resin.

2.2.4 Thermal analyses: Differential thermal analysis (T.G., DTG, and DTG)

The TG-DTA curves were obtained in an STA 449 F3 (Netzsch), using a 200 μ L α -alumina crucible with samples of about 33.5 mg. The analyses were developed at a heating rate of $10^\circ C \text{ min}^{-1}$ in a dry air atmosphere (70 mL min^{-1}) and a temperature range of $30\text{-}650^\circ C$. Therefore, we used the first derivative of the TG curve (DTG) to analyze it better. Furthermore, only three samples were analyzed (CP-00, CP-11, and CP-20).

3. Results and Discussions

Initially, the values of I , which previous authors cited, are presented because the measurement system and the four configurations are the same in this work. Then, G values for different concentrations of $CaCO_3$, the use of Equation 7 is validated for this composite case. Finally, using the same G , the samples' behavior as a function of different concentrations of $CaCO_3$ and the response of their oscillation frequency as a function of the moment of inertia is analyzed.

3.1 Measurement of the moment of inertia (I)

As mentioned in section 2.2.2, we measured the moment of inertia following the same procedure described, which resulted in the values expressed in Table 2.

We found these values using a method independent of that to determine G (section 2.2.1.)

3.2 Torsion or shear modulus results

Tables A1 and A2 provide G , f_0 , δ and Q^{-1} for the I 's values from Table 2. At the end of the article, we find the results of this section in an Appendix A.

3.3 Validating the use of Equation 7 for composite samples

We determined G for different concentrations of $CaCO_3$ in resin. An essential question arose: If the samples used are different from those of metals considered homogeneous^[28], is it valid to use Equation 7 when the internal structure of each of the specimens changed? Figure 3 was constructed based on the experimental results of Table A1, considering only diameters of 4.70 mm. Due to a possible linear post-cure shrinkage in manufactured samples (see Table 1), slight variations in diameter are critical in the calculation of G . Equation 7 shows that G 's value is inversely proportional to d^4 .

Note that in Equation 7, G is directly proportional to $L f_0^2$, and the sample diameter, d , and length, L , remain constant, maintaining an L/d ratio close to 11.32. Thus, when

Table 2. Experimental results of the rotational inertia of the pendulum.

Mass set on the pendulum rod	Rotational inertia, I (10 ⁻⁴ kg m ²)
Set 1	98.1 ± 0.5
Set 2	207 ± 1
Set 3	398 ± 1
Set 4	526 ± 4

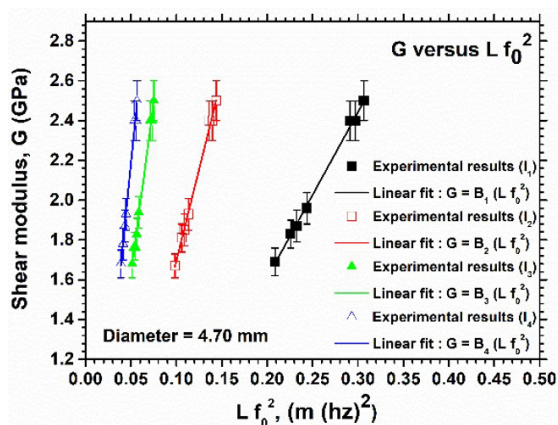


Figure 3. G versus $L f_0^2$ curves validated Equation 7. We used the samples CP-00 and CP-11 to CP-20. First, we set four inertia values (I_1, I_2, I_3 , and I_4 ; see Table 2), resulting in four curves that employ a linear adjustment. Next, we determined their angular coefficients ($B_1 = 8.3 \pm 0.9$, $B_2 = 18 \pm 2$, $B_3 = 35 \pm 4$ and $B_4 = 46 \pm 5$).

I changes the oscillation frequency value, f_0 , it also changes Lf_0^2 . For each sample, If_0^2 is practically constant. As the material changes internally, it is possible that the physical parameter δ changes as the amount of CaCO₃ increases. The parameter δ reflects the energy lost to each sample oscillation cycle^[25,26]. Therefore, it could invalidate the use of Equation 7. We determine the relationships used in Figure 3 between moments of inertia (I_i) and B_i coefficients, where $i = 1, 2, 3$, and 4. Deviations are less than 4%. Thus, Equation 7 is valid for composites.

3.4 Influence of the quantity of CaCO₃ on the torsion modulus (G)

The values of the maximum shear stress or angle-specific deformation, according to^[34,35], are

$$\tau_{MAX} = \frac{T_R d}{2 J_C} \quad (13)$$

$$\gamma_{MAX} = \frac{d \theta}{2 L} \quad (14)$$

Therefore, we express the value of G as

$$G = \frac{\tau_{MAX}}{\gamma_{MAX}} = \frac{T_R L}{J_C \theta} \quad (15)$$

Figures 4 and 5 show that G values increase with CaCO₃, T_R increases when d and L/ θ are fixed. Then, from Equation 13, it is possible to observe that the value of the maximum shear stress τ_{MAX} also increases, which alters the oscillation frequency.

Concerning G's value for a sample with the same internal structure, in Equation 15, we observe that if we fix L and θ (as we did during the experiment), for each selected d, J_C 's value does not change, and, consequently, the amount of T_R will not either. That means that T_R (resistive torque) remains the same in this situation and that G must have the same value for different inertias (see Figure 5).

The results show that the frequency values increase as the quantity of CaCO₃ increases for the equal moment of inertia, which means that τ_{MAX} rises. From the experimental results of Tables A1 and A2, we also observe that for each sample analyzed, If_0^2 is practically constant when the quantity of CaCO₃ is the same. Thus, if the torsion pendulum inertia increases, the value of f_0 must decrease. Then, if I falls, an increase of f_0 is expected. Therefore, when the quantity of CaCO₃ increases, the If_0^2 product increases (considering only samples with a diameter of 4.70 mm), corresponding to an increase in kinetic energy ($1/2 I \omega_0^2$) of oscillation and an increasingly more prominent τ_{MAX} . As shown in Figures 4 and 5, d and L/ θ are fixed, and G increases with an increasing amount of CaCO₃, so it is clear from Equation 15 that T_R increases. This change in the internal structure of the composite provides an increase in G values. However, the value of G was determined using Equation 7. Then, we changed the rotational inertia I using the same experimental conditions described above (i.e., with a fixed d and L/ θ). We observed that product If_0^2 is constant for each sample. It increases with an increasing concentration of CaCO₃ in the resin (see Tables A1 and A2). For this technique applied within the elastic range's interval, we fixed a torsion angle

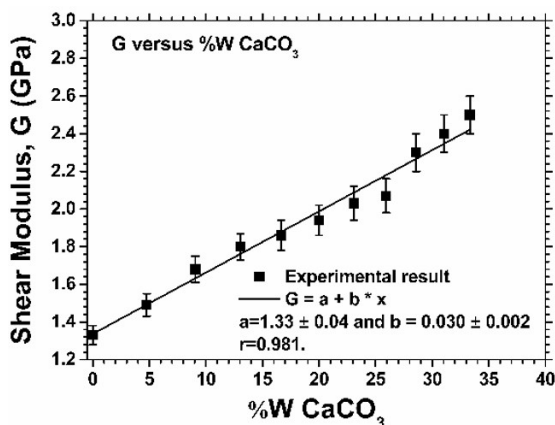


Figure 4. Curves of shear modulus G versus a percentage of CaCO₃, %W. $G = 1.33 + 0.030 (\%W)$, valid for $0 \leq \%W \leq 33.33$.

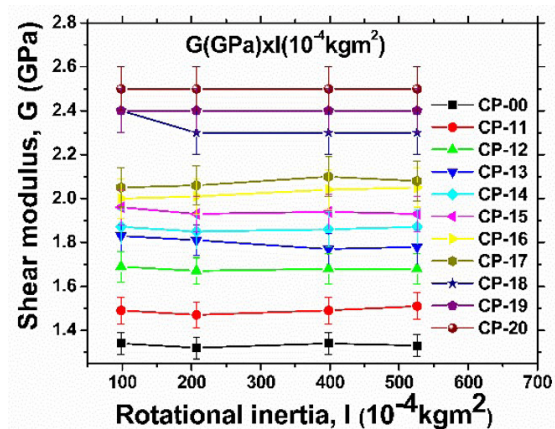


Figure 5. Curves of shear modulus G versus I. Samples: CP-00, CP-11 to CP-20.

of 1.78 degrees in the sample (corresponding to 8 degrees in the rotation sensor).

We calculated the ratio between the torsion modulus and the density after sample catalysis (G/ρ) and the respective percentages of CaCO₃. We note that G/ρ has a linear and increasing behavior, that is, $G/\rho = 1.13 + 0.03 (\%W \text{ CaCO}_3)$.

3.5 The quantity of CaCO₃ and its influence on the structures of composites (MEV)

As the percentage by weight (%W) of CaCO₃ increases, it fills a more substantial sample space, decreasing the resin amount. Because CaCO₃ adheres more actively to the resin, it can most effectively influence the shear modulus G. This can be seen from section 3.2.1 when analyzing Figures 4 and 5, where the value of G increases. The photos in Figure 6 show that at magnification scales of 500 X and 5.0 kX, CaCO₃ reduces resin volume and exhibits better adhesion, changing the G value. Because G values were more prominent than with a less significant quantity of CaCO₃, it means that CP-00, which has 100%W resin, is less

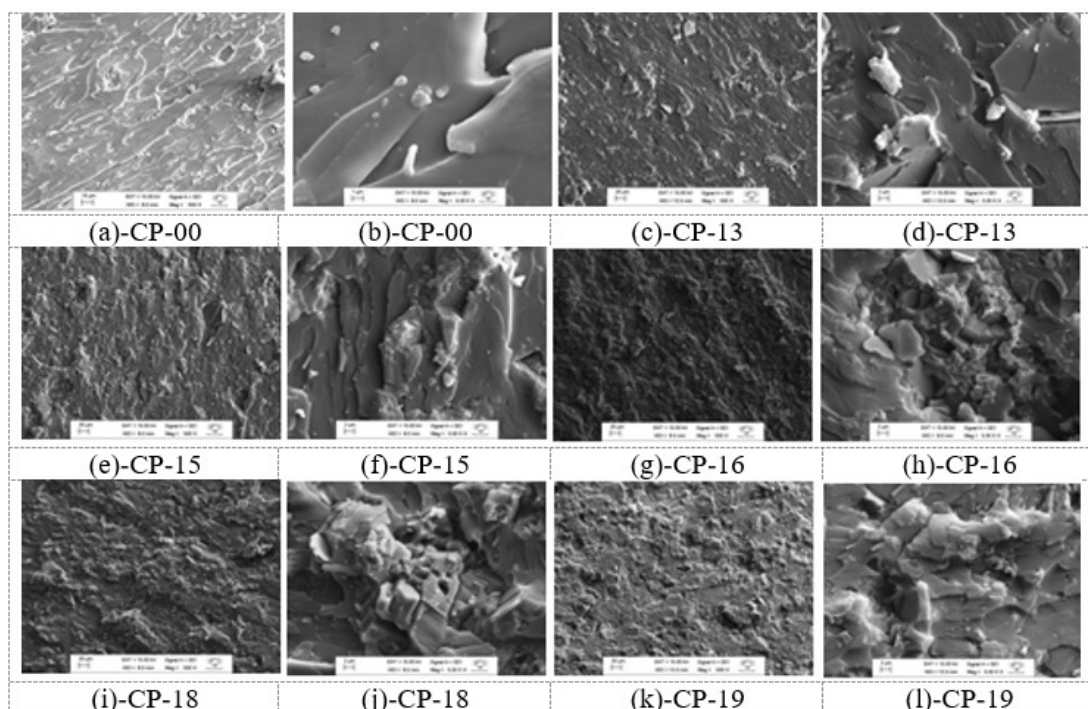


Figure 6. Photos show that CaCO_3 filler significantly reduces resin volume and improves its adhesion, which can change the G value. (a) and (b) CP-00: 100%W resin reference; (c) and (d) CP-13: 13.04%W CaCO_3 ; (e) and (f) CP-15: 20.00%W CaCO_3 ; (g) and (h) CP-16: 23.08%W CaCO_3 ; (i) and (j) CP-18: 28.57%W CaCO_3 ; (k) and (l) CP-19: 31.03%W CaCO_3 . Scales at magnification are of 500 X and 5.0 kX.

torsion-resistant than other samples. Another fact observed in CP-00 is higher total internal friction (Q^{-1}) than in the other specimens. Then, pieces that have CaCO_3 interfere with the material resistance so that the higher their %W, the higher the G value.

3.6 TG/DTG-DTA analyses

After an experimental study of the curves of the shear modulus G versus a percentage of calcium carbonate, %W, the TG/DTG-DTA curves showed the thermal stability and thermal degradation steps for CP-00, CP-11, and CP-20 (Figure 7).

In the TG curve for CP-00 (Figure 7a), we observed the thermal stability to be up to 286.4 °C; however, before reaching this value, the first step mass followed was 137.3-286.4 °C, which could be related to the evaporation of residual monomers ($\Delta m = 3.34\%$). The second step of mass loss observed is related to polymer matrix degradation, from 286.7 °C (thermal stability) to 470.4 °C ($\Delta m = 82.91\%$). This degradation step is associated with an endothermic event at 368.2 °C followed by an exotherm (369.4-433.0 °C) in the DTA curve. Moreover, the respective step exhibits a simple degradation profile by TG; however, by DTG, a complex degradation with overlapped and consecutive steps is observed. Furthermore, by DTG, the maximum degradation rate (MDR) was calculated, obtaining a value of 11.20% min^{-1} ; the MDR indicates how fast a material decomposes. Finally, the third mass loss step occurs between 433.0 °C and 607.6 °C ($\Delta m = 13.75\%$), connected with an exothermic peak

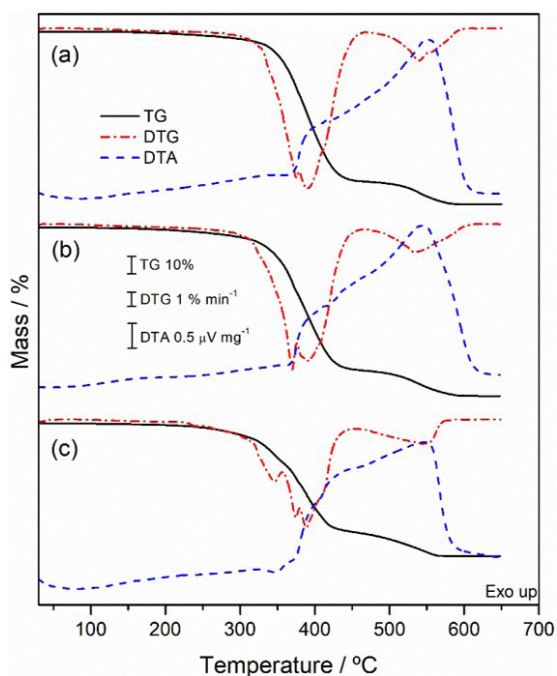


Figure 7. TG/DTG-DTA curves for (a) CP-00, (b) CP-11, and (c) CP-20.

at 551.4 °C in the DTA curve, which is related to oxidation and degradation of carbonaceous matter^[36].

Table 3. Thermal events result in each TG/DTG-DTA curve.

Samples		1st step (residual monomer releasing)	2nd step	3rd step	MDR (%min ⁻¹)**	Residual mass (%)
CP-00	θ °C	137.3-286.4	286.4-470.4	470.4-607.6	11.20	0
	Δm/%	3.34	82.91	13.75		
	T _p /°C	-	368.2 ↓; 369.4-433.0*	551.4 ↑		
CP-11	θ °C	138.0-268.2	268.3-464.7	464.7-612.5	10.20	3.34
	Δm/%	3.23	78.69	14.74		
	T _p /°C	-	366.5-419.1*	544.5 ↑		
CP-20	θ °C	137.0-286.0	286.0-440.3	440.3-569.5	7.13	23.72
	Δm/%	3.12	63.86	15.97		
	T _p /°C	-	346.2 ↓; 373.4-456.0*	546.7 ↑		

θ = temperature range; Δm = mass loss; T_p = temperature peak; ↑ = exothermic peak; * = exotherm; ↓ = endothermic peak; ** maximum degradation rate for the degradation step after thermal stability.

The TG curve for CP-11 also exhibits three mass loss steps, the first of which occurs between 138.0 °C and 268.3 °C with a mass loss equal to 3.23%. CP-11 has thermal stability (268.3 °C) lower than CP-00 (286.7 °C), indicating that adding CaCO₃ to the polymeric matrix can reduce its thermal stability. The second thermal loss related to polymer degradation occurs in the range of 268.3 °C to 464.7 °C (Δm = 78.69%), which is associated with an exotherm (366.5-419.1 °C) in the DTA curve. The MDR for the respective step is 10.20% min⁻¹, confirming that CaCO₃ addition can reduce thermal stability and MDR. The third step of mass loss (464.7-612.5 °C) is related to oxidation and degradation of remaining carbonaceous matter (Δm = 14.74%), with an exothermic peak at 544.5 °C in the DTA curve. A residue of 3.34% was present at the end of the analysis.

The TG curve for CP-20 (Figure 7c) also exhibits the first step of mass loss associated with residual monomer (1.08%), occurring between 120.3 °C and 219.6 °C. The thermal stability for the polymer was highly reduced in CP-20, indicating that high CaCO₃ concentration can spoil the thermal properties of the polymer. Therefore, the second mass loss step relates to polymeric matrix degradation, starting at 219.6 °C and ending at 454.6 °C (Δm = 61.48%). Moreover, CaCO₃ also reduces the MDR (7.13% min⁻¹). The third mass loss step occurs at 454.6-597.8 °C and is related to carbonaceous matter degradation, as observed previously. A residue of 23.72% was present at the end of the analysis.

Although adding CaCO₃ to the polymer matrix spoils the thermal stability of the polymer, the MDR value is improved. Furthermore, the addition of CaCO₃ improves the mechanical properties. These findings regarding all samples are presented in Table 3.

4. Conclusions

This study found that the torsion modulus obtained for a 100%W unsaturated polyester sample has a value of G = (1.33 ± 0.05) GPa. Different quantities of added CaCO₃ increase the G values. The highest value found was for the sample with filler of 33.33%W, at G = (2.5 ± 0.1) GPa. The dependence of G and the percentage by weight of CaCO₃ is linear, considering the studied range from 0 to

33.33%W. Finally, we can conclude this material's 21% weight gain and an 88% increase in torsion resistance. Thus, we used an equation to calculate G that does not require Poisson's ratio composites.

5. Author's Contribution

- **Conceptualization** – Carlos Alberto Fonzar Pintão; Airton Baggio; Lucas Pereira Piedade; Luiz Eduardo de Angelo Sanchez; Gilberto de Magalhães Bento Gonçalves.
- **Data curation** – 2019-2021; Carlos Alberto Fonzar Pintão.
- **Formal analysis** – Carlos Alberto Fonzar Pintão; Airton Baggio.
- **Investigation** – Carlos Alberto Fonzar Pintão; Lucas Pereira Piedade; Airton Baggio.
- **Methodology** – Carlos Alberto Fonzar Pintão.
- **Project administration** – Carlos Alberto Fonzar Pintão; Luiz Eduardo de Angelo Sanchez; Gilberto de Magalhães Bento Gonçalves.
- **Resources** – Carlos Alberto Fonzar Pintão; Airton Baggio; Luiz Eduardo de Angelo Sanchez; Gilberto de Magalhães Bento Gonçalves.
- **Software** – Carlos Alberto Fonzar Pintão.
- **Supervision** – Carlos Alberto Fonzar Pintão.
- **Validation** – Carlos Alberto Fonzar Pintão.
- **Visualization** – Carlos Alberto Fonzar Pintão.
- **Writing – original draft** – Carlos Alberto Fonzar Pintão.
- **Writing – review & editing** – Carlos Alberto Fonzar Pintão; Lucas Pereira Piedade; Airton Baggio; Luiz Eduardo de Angelo Sanchez; Gilberto de Magalhães Bento Gonçalves.

6. Acknowledgements

The authors acknowledge the Brazilian funding agencies FAPESP that the project was based on equipment

granted by FAPESP to Carlos Alberto Fonzar Pintão in 2007. #2007/04094-9; And Prof. Gilbert Bannach to perform the Thermal analysis in 2015, grant #2015/00851-6; and Capes for the postdoctoral fellowship in 2016, process number: BEX 6571/14-0. In addition, the authors thank the laboratory of polymer and thermal analysis at UNESP/Bauru for TG-DTA curves.

7. References

- Costa, A. P., Botelho, E. C., Costa, M. L., Narita, N. E., & Tarpani, J. R. (2012). A review of welding technologies for thermoplastic composites in aerospace applications. *Journal of Aerospace Technology and Management*, 4(3), 255-265. <http://dx.doi.org/10.5028/jatm.2012.040303912>.
- Bochenek, K., & Basista, M. (2015). Advances in processing of NiAl intermetallic alloys and composites for high temperature aerospace applications. *Progress in Aerospace Sciences*, 79, 136-146. <http://dx.doi.org/10.1016/j.paerosci.2015.09.003>.
- Delogu, M., Zanchi, L., Maltese, S., Bonoli, A., & Pierini, M. (2016). Environmental and economic life cycle assessment of a lightweight solution for an automotive component: A comparison between talc-filled and hollow glass microspheres-reinforced polymer composites. *Journal of Cleaner Production*, 139, 548-560. <http://dx.doi.org/10.1016/j.jclepro.2016.08.079>.
- Mouritz, A. P., Gellert, E., Burchill, P., & Challis, K. (2001). Review of advanced composite structures for naval ships and submarines. *Composite Structures*, 53(1), 21-42. [http://dx.doi.org/10.1016/S0263-8223\(00\)00175-6](http://dx.doi.org/10.1016/S0263-8223(00)00175-6).
- Francklin, H. M., Motta, L. A. C., Cunha, J., Santos, A. C., & Landim, M. V. (2019). Study of epoxy composites and sisal fibers as reinforcement of reinforced concrete structure. *IBRACON Structures and Materials Journal*, 12(2), 255-287. <http://dx.doi.org/10.1590/s1983-41952019000200004>.
- Araque, L. M., Morais, A. C. L., Alves, T. S., Azevedo, J. B., Carvalho, L. H., & Barbosa, R. (2019). Preparation and characterization of poly(hydroxybutyrate) and hollow glass microspheres composite films: Morphological, thermal, and mechanical properties. *Journal of Materials Research and Technology*, 8(1), 935-943. <http://dx.doi.org/10.1016/j.jmrt.2018.07.005>.
- Yang, H., Jiang, Y., Liu, H., Xie, D., Wan, C., Pan, H., & Jiang, S. (2018). Mechanical, thermal, and fire performance of an inorganic-organic insulation material composed of hollow glass microspheres and phenolic resin. *Journal of Colloid and Interface Science*, 530, 163-170. <http://dx.doi.org/10.1016/j.jcis.2018.06.075>. PMID:29982007.
- Shrivastava, P., Dalai, S., Sudera, P., Vijayalakshmi, S., & Sharma, P. (2014). Hollow glass microspheres as potential adjunct with orthopaedic metal implants. *Microelectronic Engineering*, 126, 103-106. <http://dx.doi.org/10.1016/j.mee.2014.06.031>.
- Kaur, M., & Singh, K. (2019). Review on titanium and titanium-based alloys as biomaterials for orthopaedic applications. *Materials Science and Engineering C*, 102, 844-862. <http://dx.doi.org/10.1016/j.msec.2019.04.064>. PMID:31147056.
- Ku, H., Wang, H., Pattarachaiyakop, N., & Trada, M. (2011). A review on the tensile properties of natural fiber reinforced polymer composites. *Composites. Part B, Engineering*, 42(4), 856-873. <http://dx.doi.org/10.1016/j.compositesb.2011.01.010>.
- Dhand, V., Mittal, G., Rhee, K. Y., Park, S.-J., & Hui, D. (2015). A short review on basalt fiber reinforced polymer composites. *Composites. Part B, Engineering*, 73, 166-180. <http://dx.doi.org/10.1016/j.compositesb.2014.12.011>.
- Sarikaya, E., Çallioglu, H., & Demirel, H. (2019). Production of epoxy composites reinforced by different natural fibers and their mechanical properties. *Composites. Part B, Engineering*, 167, 461-466. <http://dx.doi.org/10.1016/j.compositesb.2019.03.020>.
- Yang, H., Wang, X., Yu, B., Yuan, H., Song, L., Hu, Y., Yuen, R. K. K., & Yeoh, G. H. (2013). A novel polyurethane prepolymer as toughening agent: Preparation, characterization, and its influence on mechanical and flame retardant properties of phenolic foam. *Journal of Applied Polymer Science*, 128(5), 2720-2728. <http://dx.doi.org/10.1002/app.38399>.
- Kumar, N., Mireja, S., Khandelwal, V., Arun, B., & Manik, G. (2017). Lightweight high-strength hollow glass microspheres and bamboo fiber based hybrid polypropylene composite: A strength analysis and morphological study. *Composites. Part B, Engineering*, 109, 277-285. <http://dx.doi.org/10.1016/j.compositesb.2016.10.052>.
- Bartczak, Z., Argon, A. S., Cohen, R. E., & Weinberg, M. (1999). Toughness mechanism in semi-crystalline polymer blends: II. High-density polyethylene toughened with calcium carbonate filler particles. *Polymer*, 40(9), 2347-2365. [http://dx.doi.org/10.1016/S0032-3861\(98\)00444-3](http://dx.doi.org/10.1016/S0032-3861(98)00444-3).
- Sun, S., Li, C., Zhang, L., Du, H. L., & Burnell-Gray, J. S. (2006). Effects of surface modification of fumed silica on interfacial structures and mechanical properties of poly(vinyl chloride) composites. *European Polymer Journal*, 42(7), 1643-1652. <http://dx.doi.org/10.1016/j.eurpolymj.2006.01.012>.
- Zheng, J., Ozisik, R., & Siegel, R. W. (2005). Disruption of self-assembly and altered mechanical behavior in polyurethane/zinc oxide nanocomposites. *Polymer*, 46(24), 10873-10882. <http://dx.doi.org/10.1016/j.polymer.2005.08.082>.
- Zuiderduin, W. C. J., Westzaan, C., Huétink, J., & Gaymans, R. J. (2003). Toughening of polypropylene with calcium carbonate particles. *Polymer*, 44(1), 261-275. [http://dx.doi.org/10.1016/S0032-3861\(02\)00769-3](http://dx.doi.org/10.1016/S0032-3861(02)00769-3).
- He, P., Gao, Y., Lian, J., Wang, L., Qian, D., Zhao, J., Wang, W., Schulz, M. J., Zhou, X. P., & Shi, D. (2006). Surface modification and ultrasonication effect on the mechanical properties of carbon nanofiber/polycarbonate composites. *Composites. Part A, Applied Science and Manufacturing*, 37(9), 1270-1275. <http://dx.doi.org/10.1016/j.compositesa.2005.08.008>.
- Morales, E., & White, J. R. (1988). Residual stresses and molecular orientation in particulate-filled polypropylene. *Journal of Materials Science*, 23(10), 3612-3622. <http://dx.doi.org/10.1007/BF00540503>.
- Herrera-Ramirez, L. C., Cano, M., & Guzman de Villoria, R. (2017). Low thermal and high electrical conductivity in hollow glass microspheres covered with carbon nanofiber-polymer composites. *Composites Science and Technology*, 151, 211-218. <http://dx.doi.org/10.1016/j.compscitech.2017.08.020>.
- Zhang, Q.-X., Yu, Z.-Z., Xie, X. L., & Mai, Y.-W. (2004). Crystallization and impact energy of polypropylene/CaCO₃ nanocomposites with nonionic modifier. *Polymer*, 45(17), 5985-5994. <http://dx.doi.org/10.1016/j.polymer.2004.06.044>.
- Xie, X.-L., Liu, Q.-X., Li, R. K.-Y., Zhou, X.-P., Zhang, Q.-X., Yu, Z.-Z., & Mai, Y.-W. (2004). Rheological and mechanical properties of PVC/CaCO₃ nanocomposites prepared by in situ polymerization. *Polymer*, 45(19), 6665-6673. <http://dx.doi.org/10.1016/j.polymer.2004.07.045>.
- Truell, R., Elbaum, C., & Chic, B. B. (1969). *Ultrasonic methods in solid-state physics*. New York: Academic Press.
- Nowick, A. S., & Berry, B. S., editors (1972). *Anelastic relaxation in crystalline solids*. New York: Academic Press.
- Pintão, C. A. F. (2014). Measurement of the rotational inertia of bodies by using mechanical spectroscopy. *Journal of Mechanical Science and Technology*, 28(10), 4011-4020. <http://dx.doi.org/10.1007/s12206-014-0914-8>.
- Timoshenko, S. P., & Gere, J. M. (1972). *Mechanics of materials*. New York: Van Nostrand Reinhold Co.

28. Pintão, C. A. F., Correa, D. R. N., & Grandini, C. R. (2017). Torsion modulus using the technique of mechanical spectroscopy in biomaterials. *Journal of Mechanical Science and Technology*, 31(5), 2203-2211. <http://dx.doi.org/10.1007/s12206-017-0416-6>.
29. Majumdar, P., Singh, S. B., & Chakraborty, M. (2008). Elastic modulus of biomedical titanium alloys by nano-indentation and ultrasonic techniques-A comparative study. *Materials Science and Engineering A*, 489(1-2), 419-425. <http://dx.doi.org/10.1016/j.msea.2007.12.029>.
30. Piedade, L. P., Pintão, C. A. F., Foschini, C. R., Silva, M. R., & Azevedo, N. F., No. (2020). Alternative dynamic torsion test to evaluate the elastic modulus of polymers. *Materials Research Express*, 7(9), 095306. <http://dx.doi.org/10.1088/2053-1591/abb560>.
31. Pintão, C. A. F., Souza, M. P., Fo., Grandini, C. R., & Hessel, R. (2004). Experimental study of the conventional equation to determine a plate's moment of inertia. *European Journal of Physics*, 25(3), 409-417. <http://dx.doi.org/10.1088/0143-0807/25/3/008>.
32. Amrani, D. (2006). Computerized rotational system to study the moment of inertia of different objects. *European Journal of Physics*, 27(5), 1063-1069. <http://dx.doi.org/10.1088/0143-0807/27/5/005>.
33. Dedavid, B. A., Gomes, C. I., & Machado, G. (2007). *Microscopia eletrônica de varredura : aplicações e preparação de amostras : materiais poliméricos, metálicos e semicondutores*. Porto Alegre: EDIPUCRS.
34. Hibbeler, R. C. (2010). *Resistência dos materiais*. São Paulo: Pearson Prentice Hal.
35. Pintão, C. A. F., Correa, D. R. N., & Grandini, C. R. (2019). Torsion modulus as a tool to evaluate the role of thermo-mechanical treatment and composition of dental Ti-Zr alloys. *Journal of Materials Research and Technology*, 8(5), 4631-4641. <http://dx.doi.org/10.1016/j.jmrt.2019.08.007>.
36. Alarcon, R. T., Gaglieri, C., Santos, G. C., Roldao, J. C., Magdalena, A. G., Silva-Filho, L. C., & Bannach, G. (2021). A deep investigation into the thermal degradation of urethane dimethacrylate polymer. *Journal of Thermal Analysis and Calorimetry*, 147(4), 3083-3097. <http://dx.doi.org/10.1007/s10973-021-10610-y>.

Received: Mar. 15, 2022

Revised: May 27, 2022

Accepted: June 04, 2022

Appendix A – Torsion modulus results.

Table A1. Experimental result: CP-12; CP-13; CP-14; CP-15; CP-18; CP-19; CP-20. d=4.70±0.05 mm; L=53.20±0.05 mm.

I (kgm ² x10 ⁻⁴)	G(Gpa)	f ₀ (Hz)	δ	Q ⁻¹	I f ₀ ² (kgm ²)
98.1±0.5	1.69±0.07	1.98	0.171±0.005	0.00464	0.0385
207±1	1.67±0.06	1.36	0.167±0.003	0.00442	0.0383
398±1	1.68±0.07	0.982	0.168±0.002	0.00449	0.0384
526±4	1.68±0.07	0.853	0.168±0.003	0.00445	0.0383
Average I f ₀ ² value for sample CP-12:					0.0384±0.0001
98.1±0.5	1.83±0.07	2.06	0.150±0.002	0.00360	0.0416
207±1	1.81±0.07	1.41	0.152±0.004	0.00368	0.0412
398±1	1.77±0.07	1.01	0.172±0.004	0.00473	0.0406
526±4	1.78±0.08	0.880	0.173±0.002	0.00476	0.0407
Average I f ₀ ² value for sample CP-13:					0.0410±0.0005
98.1±0.5	1.87±0.08	2.09	0.188±0.007	0.00565	0.0429
207±1	1.85±0.08	1.43	0.186±0.003	0.00552	0.0423
398±1	1.86±0.08	1.03	0.200±0.001	0.00639	0.0422
526±4	1.87±0.08	0.900	0.198±0.005	0.00627	0.0426
Average I f ₀ ² value for sample CP-14:					0.0425±0.0003
98.1±0.5	1.96±0.08	2.14	0.148±0.004	0.00348	0.0449
207±1	1.93±0.08	1.46	0.145±0.002	0.00335	0.0441
398±1	1.94±0.08	1.05	0.152±0.001	0.00368	0.0439
526±4	1.93±0.08	0.915	0.150±0.002	0.00356	0.0440
Average I f ₀ ² value for sample CP-15:					0.0442±0.0005
98.1±0.5	2.4±0.1	2.34	0.151±0.006	0.00362	0.0537
207±1	2.3±0.1	1.60	0.141±0.003	0.00314	0.0530
398±1	2.3±0.1	1.16	0.139±0.001	0.00308	0.0532
526±4	2.3±0.1	1.00	0.137±0.002	0.00300	0.0530
Average I f ₀ ² value for sample CP-18:					0.0532±0.0003
98.1±0.5	2.4±0.1	2,36	0.149±0.005	0.00352	0.0548
207±1	2.4±0.1	1,62	0.145±0.001	0.00337	0.0544
398±1	2.4±0.1	1,17	0.143±0.001	0.00327	0.0549
526±4	2.4±0.1	1,02	0.140±0.003	0.00313	0.0549
Average I f ₀ ² value for sample CP-19:					0.0547±0.0002
98.1±0.5	2.5±0.1	2.40	0.17±0.01	0.0045	0.0565
207±1	2.5±0.1	1.64	0.147±0.001	0.00346	0.0560
398±1	2.5±0.1	1.19	0.155±0.001	0.00384	0.0562
526±4	2.5±0.1	1.03	0.149±0.001	0.00355	0.0558
Average I f ₀ ² value for sample CP-20:					0.0561±0.0003

Table A2. Experimental result: CP-00(d=5.00±0.05 mm); CP-11(d=4.80±0.05 mm); CP-16(d=4.80±0.05 mm); CP-17(d=4.80±0.05 mm); L=53.20±0.05 mm.

I (kgm ² x10 ⁻⁴)	G(Gpa)	f ₀ (Hz)	δ	Q ⁻¹	I f ₀ ² (kgm ²)
98.1±0.5	1.34±0.05	2.00	0.199±0.003	0.00634	0.0392
207±1	1.32±0.05	1.37	0.183±0.002	0.00530	0.0389
398±1	1.34±0.05	0.992	0.195±0.003	0.00605	0.0392
526±4	1.33±0.05	0.861	0.196±0.002	0.00611	0.0390
Average I f ₀ ² value for sample CP-00:					0.0391±0.0002
98.1±0.5	1.49±0.06	1.94	0.163±0.003	0.00423	0.0369
207±1	1.47±0.06	1.33	0.16±0.01	0.0043	0.0366
398±1	1.49±0.06	0,963	0.167±0.003	0.00443	0.0369
526±4	1.51±0.06	0.843	0.162±0.001	0.00418	0.0374
Average I f ₀ ² value for sample CP-11:					0.0370±0.0003
98.1±0.5	2.00±0.09	2.25	0.167±0.004	0.00444	0.0498
207±1	2.01±0.08	1.55	0.165±0.001	0.00433	0.0498
398±1	2.04±0.09	1.13	0.167±0.005	0.00442	0.0507
526±4	2.05±0.09	0.984	0.161±0.003	0.00410	0.0509
Average I f ₀ ² value for sample CP-16:					0.0503±0.0006
98.1±0.5	2.05±0.09	2.28	0.165±0.004	0.00433	0.0510
207±1	2.05±0.09	1.57	0.155±0.004	0.00382	0.0510
398±1	2.10±0.09	1.15	0.166±0.001	0.00441	0.0522
526±4	2.08±0.09	0.990	0.163±0.005	0.00421	0.0516
Average I f ₀ ² value for sample CP-17:					0.0514±0.0006